

QUANTIFICATION OF PIGMENTATION IN HUMAN SKIN IMAGES

Hao GONG and Michel DESVIGNES

GIPSA-Lab, Grenoble Institute of Technology, 38000, France
hao.gong, michel.desvignes@gipsa-lab.grenoble-inp.fr

ABSTRACT

In this paper, we propose and compare four different approaches for quantification of hemoglobin and melanin in skin color images. The first method is to extract erythema/melanin indices based on skin absorbance theories. The second method is based on independent component analysis (ICA) assuming that hemoglobin and melanin absorbance spectra are independent. The third method is based on non-negative matrix factorization (NMF) with multiplicative update algorithm. The fourth method is a Beer-Lambert law based model-fitting technique. Quantitative evaluation through graph-cut segmentation on melanoma indicates that model-fitting method outperforms the other three methods.

Index Terms— skin pigmentation, hemoglobin, melanin, ICA, NMF, model-fitting, graph cuts

1. INTRODUCTION

In dermatologic practice and clinical research visual cues are of primary importance for the accurate diagnosis and grading of skin lesions. However, visual inspection is subjective, at best semi-quantitative, and non-linear. In spite of the ability of human eyes to differentiate between colors (especially when contrasting colors are observed), we are unable to precisely quantify our color perception without instrumental means. Therefore, there is a need for objective, non-invasive quantification of skin pigmentation. The existing image acquisition based methods include: (a) regular color image acquisition (film or digital images) that are comprised of three broad band filtered images (red, green, and blue) approximating the light sensitivity of the cones in the human eye and (b) spectral imaging, i.e. the acquisition of a multitude of images filtered at narrow wavelength bands.

The focus of our work in this paper is to estimate hemoglobin and melanin quantitatively based on regular color imaging of skin. We propose and compare four different approaches using erythema/melanin indices, source separation algorithms (ICA and NMF) and model-fitting. Both qualitative and quantitative evaluations indicate that model-fitting approach outperforms the other three approaches.

2. MATERIALS AND METHODS

2.1. Model of Skin Optics

Fig.1 shows the schematic model of imaging process of three layered model of skin. Two predominant chromophores found in epidermal and dermal layers are melanin and hemoglobin[1]. Based on Beer-Lambert law, the absorbance of this skin model at a wavelength λ can be expressed as

$$A(\lambda) = \log(1/R(\lambda)) \\ = \epsilon_{Hb}(\lambda)l_{Hb}(\lambda)c_{Hb} + \epsilon_{Mel}(\lambda)l_{Mel}(\lambda)c_{Mel} \quad (1)$$

where l is the light penetration depth, c denotes the concentration of the chromophore and ϵ is the extinction coefficient that depends on absorbance spectrum of the chromophore (as shown in Fig.2 plotted in logarithmic scale).

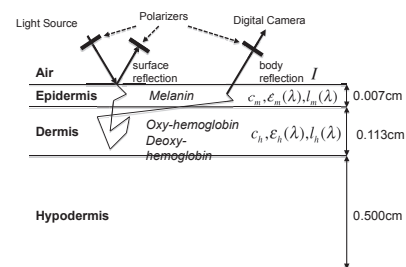


Fig. 1: Three-layered skin model.

The extinction coefficient of hemoglobin has local maxima between 542 nm and 577 nm, which provides a convenient wavelength region for the quantification of hemoglobin. The extinction coefficient of melanin has no characteristic maximum in the visible region but demonstrates a monotonic decrease towards larger wavelengths. Particularly, in red region of the spectrum (> 600 nm), the molar absorptivity of melanin is more prominent compared with the other chromophore. Hence, the red region can be used for melanin quantification.

2.2. Erythema Index and Melanin Index

Erythema index (EI) and melanin index (MI) hold excellent linearity with hemoglobin concentration and melanin

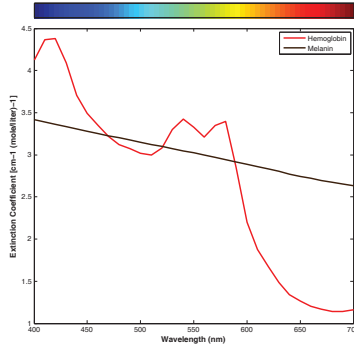


Fig. 2: Molar absorptivity spectra of chromophores.

concentration respectively. Unlike color coordinates such as $L^*a^*b^*$, the EI and MI are not indicators for evaluating 'color' but indices for quantifying the amounts of hemoglobin and melanin. Based on the theories of absorbance of skin model (Section 2.1), Takiwaki et al.[2] proposed a simple method to derive EI and MI images from RGB images. The equations for calculating EI and MI are written as follows:

$$EI = \log_{10}(1/R_{\text{green}}) - \log_{10}(1/R_{\text{red}}) \quad (2)$$

$$MI = \log_{10}(1/R_{\text{red}}) \quad (3)$$

where $R_{\text{red, green}} = S_{\text{red, green}}/W_{\text{red, green}}$. $R_{\text{red, green}}$ are the normalized red and green reflectance images of the sample under study, $S_{\text{red, green}}$ are the acquired red and green color images of the sample and $W_{\text{red, green}}$ are the average red and green values supposed to be nearly equivalent in the white standard. In fact, this method is a simplified application of algorithm proposed by Stamatas[3] within visible spectrum range.

2.3. Independent Component Analysis Based Approach

Hyvärinen et al.[4] proposed several techniques for Independent Component Analysis (ICA) for decomposing multivariate data into independent components using a function of non-Gaussianity. One of the most important contribution of their related works is the FastICA algorithm. We have applied the FastICA for our problem of skin color decomposition to quantify hemoglobin and melanin.

The general approach of ICA can be formulated as following: assume that we have a sequence of observed data x_1, x_2, \dots, x_n which can be arranged in the rows of the matrix X . If each data x_k is the linear combination of the source data (independent components) s_k then the observation matrix X can be represented as a product of two matrices

$$X = AS \quad (4)$$

where A is a mixing matrix and S is a matrix of source data. The task of ICA is to determine the mixing matrix A and the

matrix of independent source data S given the observation matrix X .

In our particular case, the application of ICA is based on independency of hemoglobin and melanin, as well as the absorbance of the multi-layered model described in Section 2.1. Here, Equation (1) can be modified in form of Equation (4):

$$\begin{bmatrix} \log(1/\mathbf{r}(\lambda_r)) \\ \log(1/\mathbf{r}(\lambda_g)) \\ \log(1/\mathbf{r}(\lambda_b)) \end{bmatrix} = \begin{bmatrix} \epsilon_h(\lambda_r) & \epsilon_m(\lambda_r) \\ \epsilon_h(\lambda_g) & \epsilon_m(\lambda_g) \\ \epsilon_h(\lambda_b) & \epsilon_m(\lambda_b) \end{bmatrix} \begin{bmatrix} \mathbf{c}_h \\ \mathbf{c}_m \end{bmatrix} \quad (5)$$

where $\mathbf{r}(\lambda_{r,g,b})$ are the normalized reflectance images of red, green and blue channel, respectively. $\epsilon_{h,m}(\lambda_{r,g,b})$ are extinction coefficients of hemoglobin and melanin at 'red band', 'green band' and 'blue band', respectively. $\mathbf{c}_{h,m}$ denote concentration distribution maps of hemoglobin and melanin. In Equation (5), we notice that the number of reflectance images (three) in observation matrix is greater than the expected number of independent components (two). Therefore, principle component analysis (PCA) is applied to reduce the dimensionality of the observation matrix and *prewhiten* the data so that the task of finding the mixing matrix reduces to the task of estimating a square orthogonal matrix.

The observation data is linearly transformed by PCA such that

$$\tilde{X} = MX = MAS = \tilde{A}S \quad (6)$$

where M is the whitening matrix calculated by eigen-value decomposition (EVD) of the covariance matrix $E\{XX^T\}$ so that $E\{\tilde{X}\tilde{X}^T\}=I$; $\tilde{A}=MA$ is a new orthogonal mixing matrix that can be seen from

$$E\{XX^T\} = \tilde{A}E\{SS^T\}\tilde{A}^T = \tilde{A}\tilde{A}^T = I \quad (7)$$

The problem is now reduce to the estimation of the orthogonal mixing matrix \tilde{A} . The columns of the matrix \tilde{A} are denoted by \tilde{a}_i and the i^{th} source component can be computed using \tilde{x} by the following equation,

$$s_i = \tilde{a}_i^T \tilde{X} = \mathbf{w}^T \tilde{X} \quad (8)$$

The Fast ICA algorithm for one unit as described in Equation (8) is

$$\mathbf{w}^+ = E\{\tilde{X}g(\mathbf{w}^T \tilde{X})\} - E\{g'(\mathbf{w}^T \tilde{X})\} \mathbf{w} \quad (9)$$

$$\mathbf{w}_{\text{new}} = \mathbf{w}^+ / \|\mathbf{w}^+\| \quad (10)$$

The one-unit algorithm can be extended to the estimation of the whole ICA transformation $S=W^T \tilde{X}$ using the Gram Schmidt deflation approach. This step of decorrelation ensures that we do not obtain the same independent component.

2.4. Non-negative Matrix Factorization Based Approach

Non-negative matrix factorization (NMF) suggested by Lee and Seung[5] is a useful method of decomposition of multivariate data. The method explicitly enforces the non-negativity constraint on the values of the source data as well

as the mixing quantities of the source data forming the mixed data.

Compared to the FastICA algorithm, NMF has two main advantages in application to our problem. First, non-negativity constraint on the source data prevents meaningless negative value of chromophore concentration. Second, no constrain on the orthogonality of the source data allows dependency between skin chromophores, which is closer to the reality.

To extend NMF in our application, we simply employ the same linear mixture model as described in Equation (4, 5). The non-negativity constraint is enforced on the source data and the mixing matrix as $\mathbf{S} \geq 0$ and $\mathbf{A} \geq 0$ respectively. Therefore, the problem can be formulated as a maximum-likelihood problem with least squares solution as in (11).

$$\mathbf{A}_{ML}, \mathbf{S}_{ML} = \arg \max_{\mathbf{A}, \mathbf{S}} p(\mathbf{X} | \mathbf{A}, \mathbf{S}) \quad (11)$$

$$\Rightarrow F = \arg \min_{\mathbf{A}, \mathbf{S}} \|\mathbf{X} - \mathbf{A}\mathbf{S}\|^2 \quad (12)$$

$$\text{Subject to : } \mathbf{A} \geq 0, \mathbf{S} \geq 0$$

In the maximum likelihood optimization, the negative log-likelihood of F is minimized i.e. $\log \|\mathbf{X} - \mathbf{A}\mathbf{S}\|$ is computed at each iteration. Here, $\|\cdot\|$ is the Euclidean norm. The updates of \mathbf{A} and \mathbf{S} can be performed under the 'multiplicative update rule' in forms as (13).

$$\mathbf{A} \leftarrow \mathbf{A} \frac{\mathbf{X}\mathbf{S}^\top}{\mathbf{A}\mathbf{S}\mathbf{S}^\top}, \quad \mathbf{S} \leftarrow \mathbf{S} \frac{\mathbf{A}^\top \mathbf{X}}{\mathbf{A}^\top \mathbf{A}\mathbf{S}} \quad (13)$$

This rule ensures the non-negative properties of the optimal solutions, \mathbf{A}_{ML} and \mathbf{S}_{ML} if the initial matrices $\mathbf{A}_{\text{initial}}$ and $\mathbf{S}_{\text{initial}}$ are strictly positive. The initialization of the source matrix \mathbf{S} is given by EI and MI and the mixing matrix \mathbf{A} can be initialized using least squares estimation with a single constraint as given in (15).

$$\mathbf{S}_{\text{initial}} = \begin{bmatrix} EI \\ MI \end{bmatrix} \quad (14)$$

$$\arg \min_{\mathbf{A}_{\text{initial}}} \|\mathbf{X} - \mathbf{A}_{\text{initial}} \mathbf{S}_{\text{initial}}\|^2 \quad (15)$$

$$\text{Subject to : } \mathbf{A}_{\text{initial}} \geq 0$$

2.5. Model-Fitting Based Approach

Source separation based approaches, like ICA and NMF, give us a statistical tool to quantify skin hemoglobin and melanin if the mixing matrix \mathbf{A} is unknown.

In this section, we employ a more accurate model which includes oxy-hemoglobin and deoxy-hemoglobin based on the oxygen-saturation of hemoglobin. So that Equation (4) can be written as

$$\begin{bmatrix} \log(1/\mathbf{T}(\lambda_r)) \\ \log(1/\mathbf{T}(\lambda_g)) \\ \log(1/\mathbf{T}(\lambda_b)) \end{bmatrix} = \begin{bmatrix} \epsilon_{\text{HbO}_2}(\lambda_r) & \epsilon_{\text{Hb}}(\lambda_r) & \epsilon_{\text{Mel}}(\lambda_r) \\ \epsilon_{\text{HbO}_2}(\lambda_g) & \epsilon_{\text{Hb}}(\lambda_g) & \epsilon_{\text{Mel}}(\lambda_g) \\ \epsilon_{\text{HbO}_2}(\lambda_b) & \epsilon_{\text{Hb}}(\lambda_b) & \epsilon_{\text{Mel}}(\lambda_b) \end{bmatrix} \begin{bmatrix} \mathbf{C}_{\text{HbO}_2} \\ \mathbf{C}_{\text{Hb}} \\ \mathbf{C}_{\text{Mel}} \end{bmatrix} \quad (16)$$

where the mixing matrix \mathbf{A} is approximated using tabulated extinction coefficients of three predominant chromophores[6, 7], $\epsilon_{\text{HbO}_2}(\lambda)$, $\epsilon_{\text{Hb}}(\lambda)$ and $\epsilon_{\text{Mel}}(\lambda)$. λ_r , λ_g and λ_b are selected at 600nm, 540nm and 440nm. Now the problem is simply to fit this model by solving a system of linear equations. Since the number of equations is equal to the number of unknowns in this linear system, we can obtain the solutions as

$$\mathbf{S} = \mathbf{A}_{\text{tabulate}}^{-1} \mathbf{X} \quad (17)$$

3. RESULTS AND DISCUSSION

In this section, we compare our NMF based and model-fitting methods to Takiwak's and ICA based methods. Firstly, we evaluate qualitatively the performances of these methods using a 'lip-pimple' image (Fig.3(a)) and a 'melanocytic nevus' image (Fig.4(a)). Based on the dermatologic knowledge that (i) lip or pimple has higher concentration of hemoglobin and lower concentration of melanin, (ii) increase of melanin content and decrease of hemoglobin content are responsible for the dark color of melanocytic nevus, one can see that model-fitting method outperforms the other three approaches in extracting relatively accurate concentration cartographies of hemoglobin and melanin. ICA based method gives poor quantitative estimations due to some unrealistic negative values of independent components. Takiwaki's method and NMF based approach give similar results though less accurate compared with model-fitting method. For example, Takiwaki's method overestimates hemoglobin concentration in nevus (Fig.4(b)) and NMF based method overestimates melanin concentration in lip (Fig.3(g)).

In context of melanoma detection, a precise and robust segmentation of skin pigmented lesion is required to discriminate tumor cell boundary and the surrounding tissue. Thus, the accuracy of the different quantification methods can be evaluated by the accuracy of the segmentation of melanoma, measured by Dice similarity coefficient (DSC), false negative ratio (FNR) and false positive ratio (FPR). We use one representative 'melanoma' image (Fig.5(a)) from the total evaluated 30 melanoma lesions to present the evaluation task. These 'melanoma' images are 938×872 pixels. The ground truth (Fig.5(b)) is obtained by manual segmentation of 5 dermatologists. First, we compare a classic graph-cut segmentation on RGB image with a modified approach on five-level images: RGB and Hemoglobin/Melanin images. It will be demonstrated below that by adding Hemoglobin/Melanin images to RGB image, graph-cut segmentation gives better result. Second, we compare the modified graph-cut segmentations obtained by different quantification methods. In Table 1, we can observe how model-fitting method achieves better results. The DSC is increased to 0.982 while both FNR and FPR decrease. NMF based method and Takiwaki's method give similar results, which is exactly the same as for the qualitative evaluation.

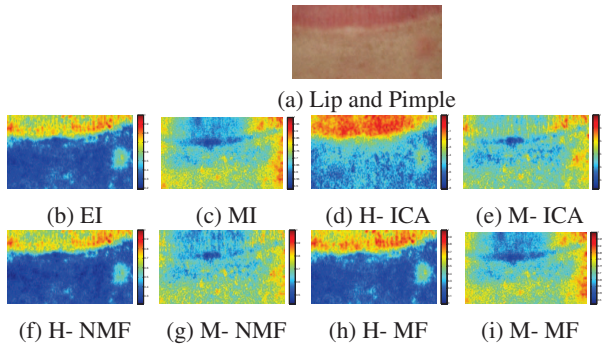


Fig. 3: Comparison of hemoglobin and melanin concentration cartographies on 'lip-pimple'. 'H': hemoglobin. 'M': melanin. 'MF': model-fitting.

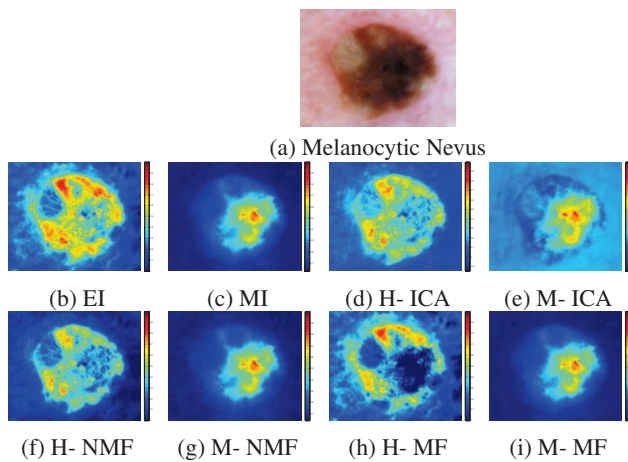


Fig. 4: Comparison of hemoglobin and melanin concentration cartographies on 'melanocytic nevus'.

4. CONCLUSIONS

In this paper, we propose and compare four different quantitative estimation approaches on skin color image using erythema/melanin indices, source separation algorithms (ICA and NMF) and model-fitting. By means of two comparative experiments based on dermatologic knowledge and graph-cut segmentation, model-fitting approach obtains more accurate quantitative estimation of skin hemoglobin and melanin. In future work, multi-spectral imaging based approaches will be studied.

5. REFERENCES

[1] R. Rox Anderson and John A. Parrish, "The optics of human skin," *J Invest Dermatol*, vol. 77, no. 1, pp. 13–19, 1981.

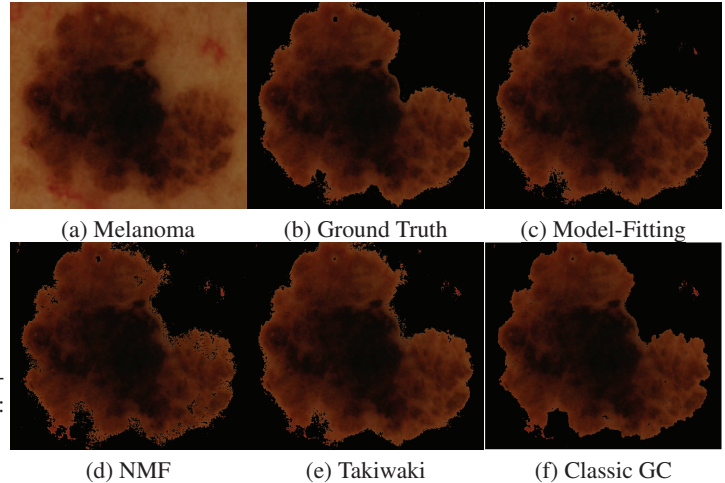


Fig. 5: Comparison of segmentation results on 'melanoma'. 'GC': graph-cut.

Table 1: Comparison of Segmentation Accuracy

| | Model-Fitting | NMF | Takiwaki | ICA | Classic GC |
|-----|---------------|-------|----------|-------|------------|
| DSC | 0.982 | 0.967 | 0.971 | 0.954 | 0.965 |
| FNR | 0.013 | 0.044 | 0.012 | 0.059 | 0.061 |
| FPR | 0.023 | 0.024 | 0.027 | 0.031 | 0.028 |

[2] Tadamasu Yamamoto, Hirotsugu Takiwaki, and Hiroshi Ohshima, "Derivation and clinical application of special imaging by means of digital cameras and image j free-ware for quantification of erythema and pigmentation," *Skin Research and Technology*, vol. 14, no. 1, pp. 26–34, 2008.

[3] Georgios N. Stamatias, Barbara Z. Zmudzka, and Niki-foros Kollias, "Non-invasive measurements of skin pigmentation in situ," *Pigment Cell Research*, vol. 17, no. 6, pp. 618–626, 2004.

[4] Aapo Hyvärinen and Erkki Oja, "A fast fixed-point algorithm for independent component analysis," *Neural Computation*, vol. 9, no. 7, pp. 1483–1492, 1997.

[5] Daniel D. Lee and H. Sebastian Seung, "Learning the parts of objects by non-negative matrix factorization learning the parts of objects by non-negative matrix factorization," *Nature*, vol. 401, pp. 788–791, 1999.

[6] Scott Prahl, "Tabulated molar extinction coefficient for hemoglobin in water," <http://omlc.ogi.edu/spectra/hemoglobin/summary.html>.

[7] Steven Jacques, "Extinction coefficient of melanin," <http://omlc.ogi.edu/spectra/melanin/eumelanin.html>.